Dalton Transactions

PAPER

View Article Online
View Journal | View Issue

Cite this: *Dalton Trans.*, 2018, **47**, 14293

Metallosomes for biomedical applications by mixing molybdenum carbonyl metallosurfactants and phospholipids†

M. Marín-García, [a] N. Benseny-Cases, [b] M. Camacho, [c] Y. Perrie,[d] J. Suades *[e] and R. Barnadas-Rodríguez *[a]

New supramolecular systems have been prepared by mixing molybdenum organometallic metallosurfactants $M(CO)_5L$ and $M(CO)_4L_2$ {L = $Ph_2P(CH_2)_6SO_3Na$} with the phospholipid phosphatidylcholine. The analysis of the resulting supramolecular structures using dynamic light scattering and cryo-transmission electron microscopy has shown the formation of different aggregates depending on the metallosurfactant/phospholipid ratio, as well as a significantly different behaviour between the two studied metallosurfactants. Mixed vesicles, with properties very similar to liposomes, can be obtained with both compounds, and are called metallosomes. The formation of the mixed aggregates has also been studied by microfluidics using MeOH and EtOH as organic solvents, and it has been observed that the size of the aggregates is strongly dependent on the organic solvent used. In order to analyse the viability of these mixed systems as CO Releasing Molecules (CORMs) for biomedical applications, the CO release was studied by FT-IR spectroscopy, showing that they behave as photo-CORMs with visible and ultraviolet light. Toxicity studies of the different mixed aggregate systems have shown that metallosomes exhibit a very low toxicity, similar to liposomes that do not contain metallosurfactants, which is well below the results observed for pure metallosurfactants. Micro-FTIR microscopy using synchrotron radiation has shown the presence of metallosurfactants in cells. The results of this study show the influence of the length of the hydrocarbon chain on the properties of these mixed systems, compared with previously reported data.

Received 20th April 2018,
Accepted 15th June 2018

DOI: 10.1039/c8dt01584h

rsc.li/dalton

Introduction

The first references to the concept "metallosurfactant" (MTS) were published in the 1990s and, in general, this term was used to refer to molecules that behave as surfactants and contain a metal atom in the molecular structure.[1] Since amphiphilic molecules with surfactant properties can help obtain supramolecular structures by self-assembly in an aqueous solution, this simple concept can also obtain supramolecular structures with metallic atoms. This is an attractive idea that has been studied with a broad range of different aims (anticancer agents,[2] antimicrobial compounds,[2,3] catalysis,[4] corrosion mitigation,[5] labelling phospholipid membranes,[6] light-driven hydrogen generation,[7] magnetic resonance imaging,[8] metallomesogens,[9] nanoparticles,[10] optoelectronic devices,[11] and templates for mesoporous materials[12]) as well as being reviewed from different points of view.[13]

Since surfactants are amphiphilic molecules that contain hydrophobic groups and a polar group, and considering that in a wide range of metal complexes the resulting coordinated metal atom is located in a polar region of the molecule, in a large number of the reported MTSs the metal atom is placed in the polar head group of the surfactants. This is the case for metallic complexes with alkyl amines or organic carboxylates that contain a long hydrophobic chain (which can be seen schematically in the drawing (a) of Scheme 1). Thus, a large number of the reported MTSs fit this representation in which the metal atom is located in the polar group of the amphiphilic molecule. However, other designs are possible, and exactly the opposite situation is shown in the drawing (b) of

[a]*Biophysics Unit/Center for Biophysical Studies, Department of Biochemistry and Molecular Biology, Faculty of Medicine, Universitat Autònoma de Barcelona, Avda. de Can Domènech, 08193 Cerdanyola, Spain. E-mail: Ramon.Barnadas@uab.cat*
[b]*ALBA Synchrotron, Carrer de la Llum 2-26, 08290 Cerdanyola, Spain*
[c]*Laboratory of Angiology, Vascular Biology and Inflammation/Institute of Biomedical Research, Hospital de la Santa Creu i de Sant Pau, Universitat Autònoma de Barcelona, Sant Antoni Maria Claret, 167, 08025 Barcelona, Spain*
[d]*Strathclyde Institute of Pharmacy and Biomedical Sciences, University of Strathclyde, Glasgow G4 0RE, UK*
[e]*Departament de Química, Edifici C, Universitat Autònoma de Barcelona, 08193 Cerdanyola, Spain. E-mail: Joan.Suades@uab.cat*

†Electronic supplementary information (ESI) available. See DOI: 10.1039/c8dt01584h

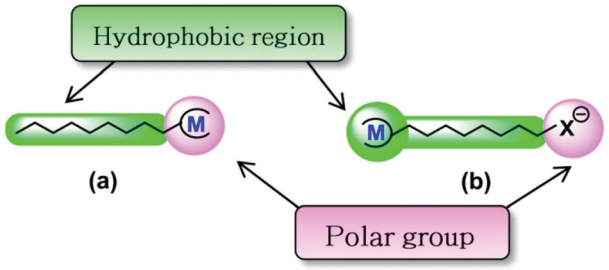

Scheme 1 Representation of metallosurfactants with the metal (M) in the polar head group (a) or in the hydrophobic region (b).

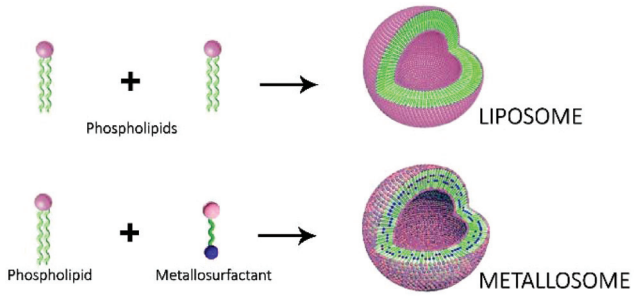

Scheme 2 Formation of liposomes with phospholipids or metallosomes by mixing metallosurfactants and phospholipids.

Scheme 1 (an MTS that contains the metal atom embedded in the hydrophobic tail). These kinds of compounds can be prepared by means of an organometallic approach, because it makes it possible to locate a metallic atom in a hydrophobic environment. Although these MTSs are much less common, some examples have been reported, such as the ferrocenyl surfactants.[14] Following this approach, we undertook the study of MTSs with metal carbonyls,[15,16] since their non-polar properties allow the metallic atom to be placed in the hydrophobic region of the MTSs. The self-assembly of these compounds can lead to supramolecular systems with metal carbonyls and, from their broad range of possible applications, we chose to focus on the study of these supramolecular metal carbonyls as CO releasing molecules (CORMs) for biomedical applications. Thus, we demonstrate that molybdenum carbonyls with the phosphine ligands $Ph_2P(CH_2)_nSO_3Na$ {n = 2 (L2), 6 (L6), 10 (L10)} form vesicular aggregates in aqueous media and these supramolecular systems can act as CO releasing molecules {$Mo(CO)_4L_2$ and $Mo(CO)_5L$; L = L2, L6, L10}. However, a problematic point for a possible application of these compounds in medicine is that the supramolecular arrangements formed by these MTSs are labile systems and they lead to different kinds of aggregates depending on the concentration of MTSs, and dilution causes disaggregation of vesicles. In order to improve the properties of these supramolecular systems for biomedical applications, we undertook the study of mixed systems of MTSs and phospholipids. In a recent communication[17] we showed that, in contrast to the aggregates formed by pure MTSs, mixed systems of MTSs and phospholipids lead to vesicular aggregates, very similar to liposomes, which are stable under dilution. These new systems can be named metallosomes, because they are vesicles with entrapped water, and their membrane is analogous to the classical lipid bilayer (Scheme 2). They exhibit properties very similar to those of liposomes, as stability under dilution, and size control using standard methods such as extrusion. Furthermore, it should be highlighted that the most interesting result of this study was to establish that the toxicity of metallosomes is at least ten-fold lower than that of the MTS aggregates without phospholipids. As far as we know, only a very limited number of aggregates classified as metallosomes have been reported,[18] most of them aimed as possible biomedical applications.

In our previous communication were reported the preliminary results of our work with metallosomes, which was limited to molybdenum complexes with the ligand with the shortest hydrocarbon chain (L2), $Mo(CO)_4(L2)_2$ (TCOL2) and $Mo(CO)_5(L2)$ (PCOL2). In the present paper, the study has been extended to metal complexes with the ligand L6 {$Mo(CO)_4(L6)_2$ (TCOL6) and Mo(CO)5(L6) (PCOL6)} in order to analyse the influence of the length of the hydrocarbon chain of the ligand on the metallosome properties.

Results and discussion

Structures of the mixed aggregates obtained by the film hydration method

The formation of binary mixed structures composed of an MTS with 6 carbon atoms in the hydrocarbon chains (PCOL6 or TCOL6) and soy phosphatidylcholine (SPC) was studied by hydrating and vortexing a homogeneous dry thin film of the substances prepared by rotary evaporation of an organic solution. The SPC concentration of the suspensions was kept constant at 3 mM while the MTS concentration ranged from 0 to 10 mM. Dynamic light scattering (DLS) analysis shows (Fig. 1) a different effect of both MTSs on the type of aggregate

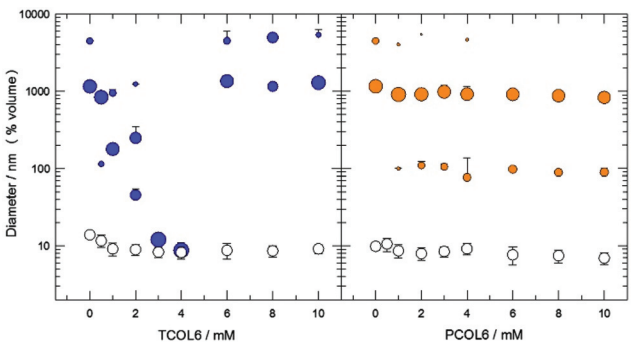

Fig. 1 DLS analysis of the size distribution of TCOL6/SPC aggregates (blue) and PCOL6/SPC aggregates (orange) as a function of the concentration of each MTS (mean ± std. dev.; $n \geq 3$). White circles correspond to aggregates obtained after addition of Triton X-100. The SPC concentration was kept constant (3 mM). The area of the circles is proportional to the percentage of aggregates of a given diameter.

formed. For the case of the MTS bearing 2 hydrocarbon chains, TCOL6, its progressive concentration increase from 0 to 4 mM produces a concomitant decrease in the size of the structures formed. As can be observed, the size of the aggregates changes more than 2 orders of magnitude: initial liposomes obtained with no MTS are of about 1 μm in diameter; TCOL6 incorporation between 0.5 and 2 mM still renders structures located in the vesicle domain but with a smaller size; and, finally, in the 3 to 4 mM nanometre range, structures of approximately 8 nm are detected. If Triton X-100 is added to the suspensions at a solubilising concentration (10 mM), vesicles are totally disrupted and mixed micelles of about 8 nm are obtained. However, when the surfactant is added to the small aggregates no significant change of the size is observed. Surprisingly, at a TCOL6 concentration higher than 4 mM there is a sharp increase of the size and micrometre sized aggregates, which sediment in a few minutes, are detected, part of them having a size located at the higher limit of detection of the device (6.5 μm). The evolution of the system is quite different for the case of PCOL6/SPC mixtures: apparently there are no remarkable changes in the vesicle size. Incorporation of TCOL6 into the SPC phospholipid bilayers only causes the formation of vesicles of about 90–100 nm, but the main population is maintained close to the initial size of the pure SPC liposomes, at approximately 1000 nm. As for the case of TCOL6, addition of Triton X-100 also causes total vesicle disruption.

The morphology of all the previously described systems was studied by cryo-TEM and optical microscopy. As can be observed (Fig. 2A and B), at a low concentration of TCOL6 the mixed vesicles are mostly uni- and oligo-lamellar, and show a smooth and regular membrane. Some of these vesicles exhibit a central dark area, which is indicative of their protruding out of the vitrified film (thickness about 10 to 500 nm).[19] Between 3 and 4 mM of TCOL6 very small aggregates are observed, with some of them having the shape of a disk or a bar (Fig. 2C). The presence of both shapes can be explained by the formation of bicelles, that is, small fragments of SPC bilayers forming a circular disc surrounded by a rim of a short-chain surfactant, in our case, TCOL6. Orientation of the former aggregates in the vitrified samples allows the observation of both thin bars and small disks when they lie perpendicular or parallel to the grid, respectively.[19] As regards the samples with a TCOL6 concentration greater than 4 mM, no large aggregates were visible by cryo-TEM, although very large rods were observed by optical microscopy (Fig. 2D). This fact may be a consequence of the sample treatment for cryo-TEM analysis: very large structures are usually removed from the grid during

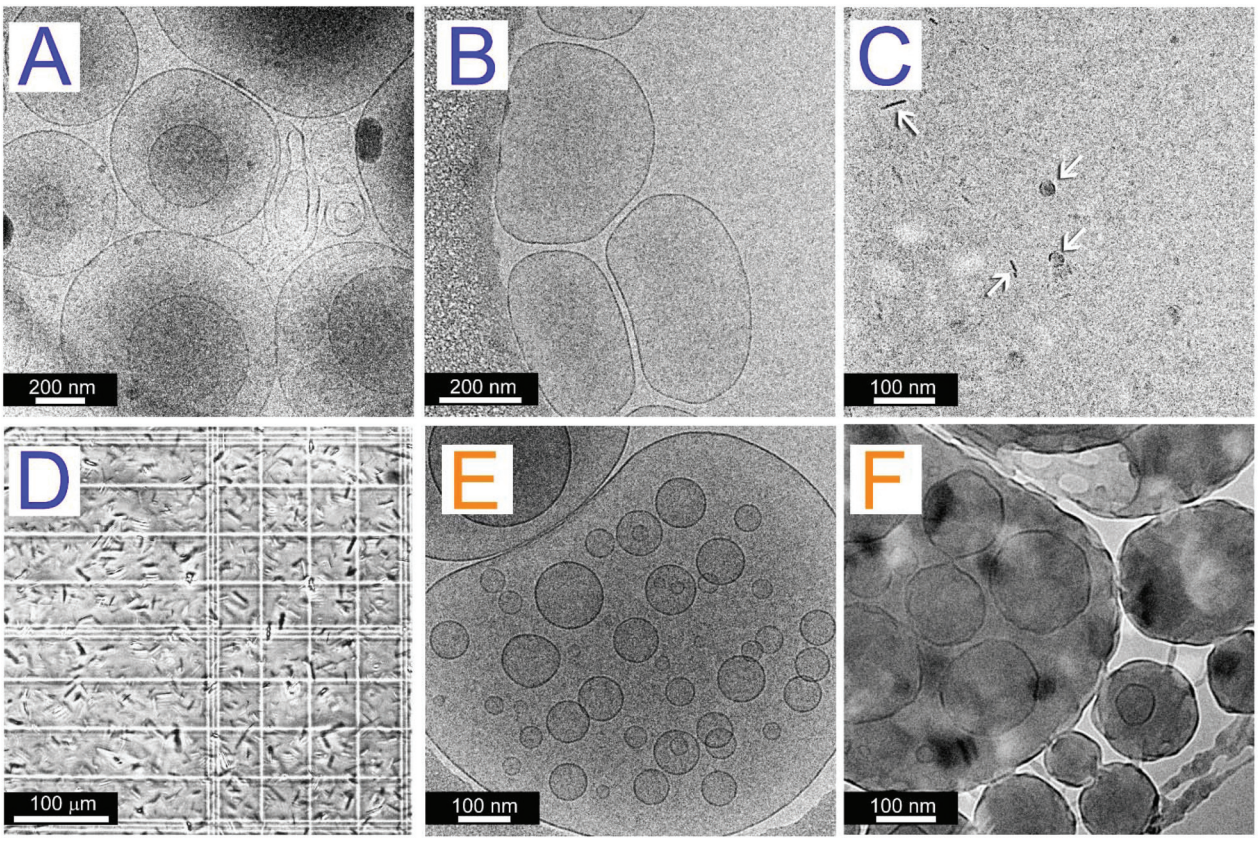

Fig. 2 Images of mixed systems of MTS and SPC. A and B: Cryo-TEM pictures of TCOL6/SPC 1 : 3 mM/mM vesicles. C: Cryo-TEM image of TCOL6/SPC 3 : 3 mM/mM bicelles (arrows). D: Optical microscopy picture of TCOL6/SPC 10 : 3 mM/mM rods. E and F: Cryo-TEM images of PCOL6/SPC vesicles at 6 : 3 and 10 : 3 mM/mM, respectively.

the blotting process, since they protrude far too much due to the thickness of the water film. The structure of PCOL6/SPC aggregates was quite different from that of the TCOL6/SPC ones. On the one hand, when a PCOL6/SPC ratio of 3 : 6 mM/mM was reached, small vesicles and also micrometric multivesicular (Fig. 2E) and multi-lamellar vesicles (MLVs) were observed. In all cases, they exhibit the same smooth membrane as TCOL6/SPC aggregates. On the other hand, when the relative amount of MTS increases, vesicles are deformed, show a rough membrane and furthermore, branched thread-like micelles connected to the vesicles appear, as can be seen in Fig. 2F for PCOL6/SPC 10 : 3 mM/mM.

Habitually, one required characteristic of aggregated systems intended for biomedical applications is their stability upon dilution. This is important, because their structure should be preserved once they are in the fluid biological media, otherwise their cargo would be disseminated in a non-specific manner during their journey to their target. Knowing that pure MTSs are not stable upon dilution, the stability of mixed vesicles and bicelles was monitored by DLS, by performing progressive dilutions of initial concentrated samples. The results show that both vesicles and bicelles of TCOL6/SPC were stable upon dilution for at least two orders of magnitude, since no significant change was observed in the mean diameter (Fig. 3). Positive and negative controls were a bicellar suspension of phospholipids and pure SPC liposomes, respectively (Fig. S1, ESI†). In contrast, PCOL6/SPC systems showed a different behaviour compared to TCOL6/SPC ones. While vesicles with a high content of SPC showed no change of the vesicle size upon dilution (Fig. 3), those with a low SPC content were non-stable (NS) and showed a decrease in the diameter (from about 700 nm to 250 nm) when progressively diluted 100 times. Since it is known that SPC membranes are not altered by dilution, this phenomenon has to be a consequence of the release of PCOL6 from the mixed aggregates when the equilibrium between the free and the vesicular MTS is modified. Note that the diameter change is more intense at a PCOL6 concentration of about 1.2 mM (normalised concentration 0.1; initial concentration of the system 12 : 3.6 mM/mM PCOL6/SPC), that is, the critical micellar concentration of PCOL6.[15,16]

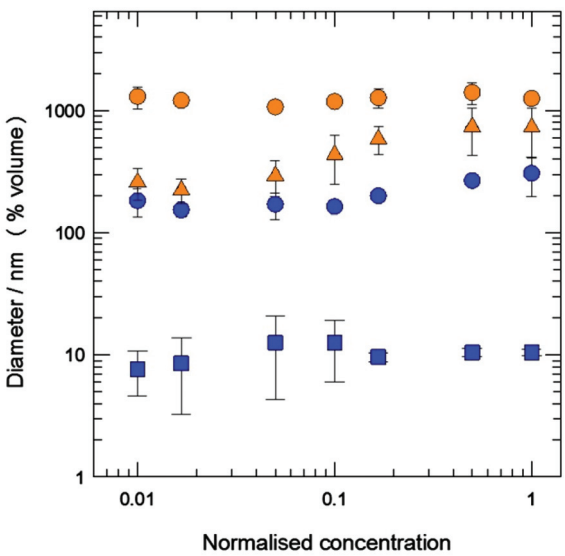

Fig. 3 Stability of MTS/SPC aggregates upon dilution: TCOL6/SPC 12 : 36 mM/mM (blue circles); TCOL6/SPC 12 : 12 mM/mM bicelles (blue squares); PCOL6/SPC 12 : 36 mM/mM vesicles (orange circles); and PCOL6/SPC 12 : 3.6 m/mM non-sable vesicles (orange triangles). Previous concentrations correspond to the initial concentrations (normalised concentration = 1). Mean ± std. dev.; $n \geq 2$.

It can be observed that sizes measured by DLS match with those observed by cryo-TEM, especially for submicron vesicles which are well within the detection range of both techniques. It is apparent that despite the difference in the length and shape between both MTS and SPC, hydration of binary films allows the spontaneous formation of mixed aggregates. This fact parallels the behaviour of the mixtures of PCOL2 and TCOL2 with SPC, which also form aggregates,[17] even though the length of their hydrocarbon chains (2 methylene groups) is one-third those of PCOL6 and TCOL6. Thus, the known capacity of phospholipid fatty acid chains for filling (by rotation) the gaps generated inside the bilayers caused by the inclusion of short and bulky molecules should explain the formation of mixed vesicles.

However, it should be highlighted that some significant differences were found between the aggregates formed by the molybdenum complexes of the L2 and L6 families. For the case of TCOL6/SPC mixtures, when the relative amount of MTS is too high, membranes destabilise and other structures are formed (first bicelles and, finally, very large rods). Both aggregates were not observed with TCOL2, since only micelles were obtained at high MTS/SPC ratios. The evolution of the PCOL6/SPC systems is also quite different from that of the PCOL2/SPC systems, where a progressive decrease of the aggregate size is observed upon the increase of the MTS/SPC ratio and micelles are obtained. This is not the case for PCOL6, and a progressive overloading of the membranes takes place at high PCOL6 to SPC ratios. The presence of very dark vesicles indicates the extreme protrusion of these aggregates out of the film, consistent with a very big size, which is not detected by DLS since it is far away from its upper limit of detection. Moreover, the vesicle deformation and the roughness of the membrane (Fig. 2F) are indicative of the difficult packing of the vesicular membranes, which tend to form thread-like structures and showed instability upon dilution. Vesicle deformation have been observed in other binary systems as, for example distearoylphosphatidylcholine/cholesterol liposomes at a 60/40 molar ratio.[20] This cholesterol content is close to that which causes formation of tubular liposomes, possibly caused by the formation of phase domains into the bilayer.

Structure of the mixed aggregates obtained by microfluidics

During their preparation, the characteristics of surfactant aggregates can be controlled by several factors, such as the concentration of organic solvents, ionic strength, temperature,

or shear stress.[21] Some of the former factors are involved in the microfluidic process, technology used to obtain different types of drug delivery systems,[22] a reason why their effect on the formation of mixed MTS vesicles was studied. Tables included in Fig. 4 show the experimental results for the level combinations of the Total Flow Rate (TFR) and the water to solvent (methanol or ethanol) Flow Rate Ratio (FRR) for the PCOL6/SPC 1 : 3 mM/mM system. The corresponding fitted surfaces of response are shown (other results are shown in Fig. S2, ESI†). As can be observed, the size of the aggregates clearly depends on the type of organic solvent used: at any given combination of TFR and FRR, the size of the aggregates when using methanol is always smaller than that obtained when the solvent used is ethanol. Regarding the effect of the total and relative flows, TFR and FRR have a big influence on the size when methanol is used, while only FRR is the main factor when the solvent used is ethanol. The study of the influence of ionic strength (between 0 and 155 mM of NaCl) was carried out at several TFR values (2, 10 and 18 mL min^{-1}) and by fixing the solvent (methanol) and the FRR (at 3). Results for the PCOL6/SPC 1 : 3 mM/mM system are shown in Fig. 5 (see results for the TCOL6/SPC 1 : 3 mM/mM system in Fig. S3, ESI†) and as can be observed there is a concomitant increase of the ionic strength and the size of the vesicles at any of the TFRs assayed. Finally, the morphology of big PCOL6/SPC vesicles corresponds to multi-lamellar structures (Fig. 6), which is highly different from that obtained by the film method (Fig. 2).

The previously expressed results can be compared with those obtained by other authors when phospholipid liposomes are prepared using isopropanol or ethanol as the solvent. In these cases, the general finding is that the FRR is a major factor in regulating liposome size, with both variables being

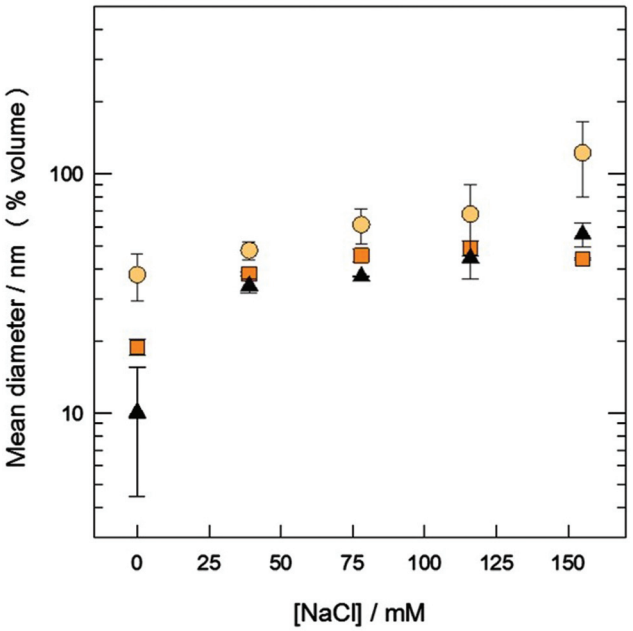

Fig. 5 Mean diameter of PCOL6/SPC 1 : 3 mM/mM vesicles obtained by microfluidics as a function of the ionic strength of the aqueous medium, using methanol as the solvent, FRR = 3, and TFR = 2 (circles), 10 (squares) and 18 mL min^{-1} (triangles). Mean ± std. dev.; $n \geq 2$.

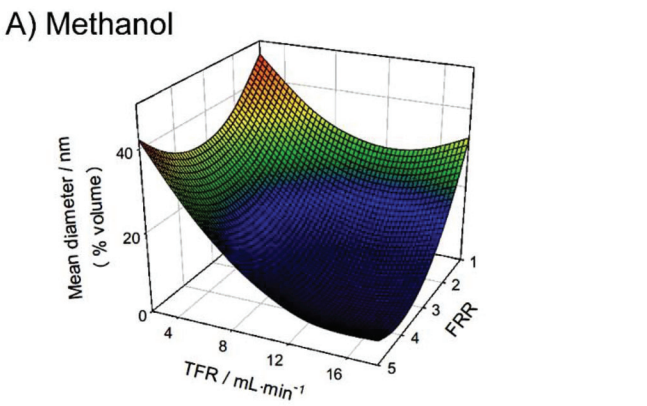

Mean diameter / nm (% volume)

FRR \ TFR (mL· min^{-1})	2	6	10	14	18
1	42.6 ± 0.01		32.4 ± 0.6		28.0 ± 0.91
2		22.6 ± 2.48		18.0 ± 1.76	
3	33.9 ± 8.72		8.69 ± 1.87		6.06 ± 1.97
4		13.3 ± 1.93		4.74 ± 0.09	
5	46.6 ± 3.97		8.24 ± 1.31		9.88 ± 7.11

Diameter (mm) = -8.23-3.89·FRR-6.24·TFR+2.98·FRR^2+2.92·TFR^2-1.38·FRR·TFR
r^2 = 0.89; standard error = 5.01

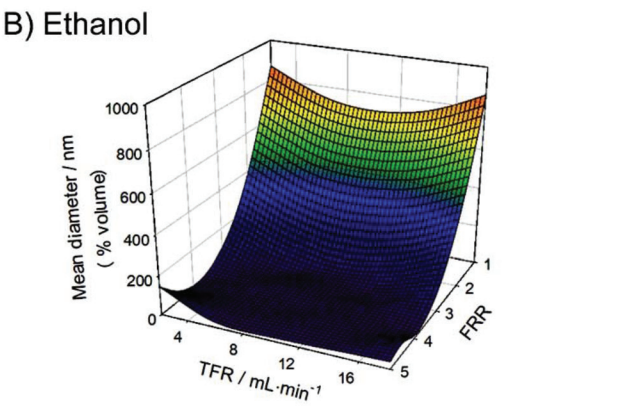

Mean diameter / nm (% volume)

FRR \ TFR (mL· min^{-1})	2	6	10	14	18
1	1033 ± 357		653 ± 141		986 ± 292
2		658 ± 21.1		42.0 ± 8.17	
3	148 ± 62.0		27.5 ± 2.47		22.3 ± 4.74
4		26.2 ± 4.48		4.74 ± 0.09	
5	68.0 ± 12.1		18.8 ± 2.43		20.6 ± 1.52

Diameter (mm) = -61.2-181·FRR+103·FRR^2+38.8·TFR^2
r^2 = 0.83; standard error = 160

Fig. 4 Mean diameter of PCOL6/SPC 1 : 3 mM/mM vesicles obtained by microfluidics using methanol (A) or ethanol (B) as the solvent as a function of the Flow Rate Ratio (FRR) and the Total Flow Rate (TFR). Fitted surface responses obtained from the experimental points are given (mean ± std. dev.; $n \geq 2$).

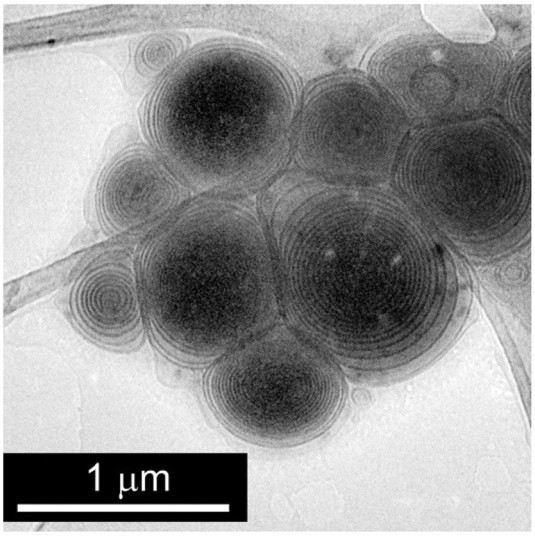

Fig. 6 Cryo-TEM picture of PCOL6/SPC 1 : 3 mM/mM vesicles obtained by microfluidics using ethanol as the solvent at TFR = 10 mL min^{-1} and FRR = 1.

inversely related.[23] This effect is a consequence of the drop in the final solvent concentration due to the FRR increase, which reduces liposome fusion.[24] Vesicle fusion, like many other alterations of membrane properties (such as permeability, surface tension, and area per molecule),[25] is driven by alcohol insertion into phospholipid bilayers. In this sense, MTS/SPC vesicular systems exhibit a behaviour analogous to that of liposomes, since any FFR increase, using either methanol or ethanol as solvent, causes a decrease in the vesicle size. On the other hand, there is a big difference in the vesicle size range depending on the solvent used. Observe that while vesicles obtained in the presence of the shortest chain alcohol (methanol) are always located at the domain of the small unilamellar vesicles (SUVs) with, for example, a maximum diameter of about 50 nm at TFR = 2 and FRR = 1, those obtained in the presence of ethanol range from SUVs to MLVs, and achieve micrometre size under the former stated conditions. This noticeable difference can be a consequence of the difference in the fusogenic activity exhibited by alcohols depending on their chain length. Paxman *et al.*[26] found that those alcohols with 2 to 4 carbon atoms increase vesicle fusion to planar bilayers, and that methanol inhibits it. This could explain why vesicles obtained by microfluidics in the presence of methanol should preserve their small size and those, contrarily, with a high content of ethanol (low FRR) in the bulk should fuse and yield large multi-layered vesicles, as observed by cryo-TEM (Fig. 6).

CO release from mixed aggregated systems upon irradiation

TCOL6 and PCOL6 (and their derived mixed aggregates), which contain an Mo atom linked to several CO groups, not only have a very particular structure because of their hydrophobic domain, but also encompass the possibility to become CO releasing molecules (CORMs). Previous studies carried out with MTSs with shorter chains (2 carbon atoms, *i.e.*, TCOL2 and PCOL2) demonstrated that they are stable in the dark, and that UVA and visible irradiations trigger CO release as gas.[17] This capability shows that, in fact, these molecules are photo-CORMs, and that their different mixed aggregated structures can be used as drug (CO) delivery systems with potential biomedical applications.[27]

With these precedents, the CO releasing properties of TCOL6 and PCOL6 mixed systems were studied and the results are shown in Fig. 7A and B. The FTIR spectra monitors the decrease of the infrared CO absorption bands of both molecules under UVA light (λ_{max} = 365 nm). The insets of Fig. 7

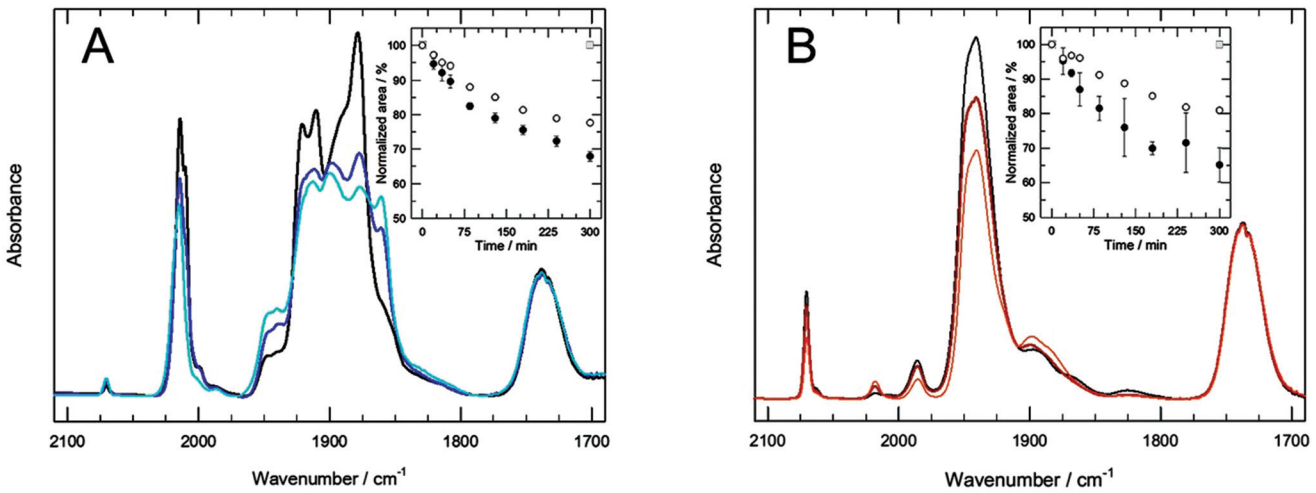

Fig. 7 Infrared spectra of (A) TCOL6/SPC 10 : 10 mM/mM and (B) PCOL6/SPC 10 : 30 mM/mM under irradiation with UVA (365 nm) at different times. Inset A: Changes in the relative area of the peak at 2017 cm^{-1} of TCOL6/SPC aggregates upon illumination with UVA (black) or visible light (blue). Inset B: Changes in the relative area of the peak at 2070 cm^{-1} of PCOL6/SPC aggregates upon illumination with UVA (black circles), visible light (white circles) or kept in the dark (grey squares). Mean ± std. dev.; n = 2.

show the relative changes of the 2017 cm^{-1} and 2070 cm^{-1} bands for TCOL6 and PCOL6, respectively, with UVA or visible irradiation. For a given MTS and type of light, there were no significant differences between the diverse aggregated systems, a reason why their results are shown in a single plot. As can be observed, TCOL6 and PCOL6 are photo-CORMs, with UVA being the most effective light to deliver CO. However, note that visible light is also active, as it was for TCOL2 and PCOL2. The parallel behaviour of both families of MTS indicates that the length of the hydrocarbon chain has no effect on their CO releasing capability.

Toxicity of MTS aggregates on human fibroblast cell cultures

Toxicity assays were carried out for the different mixed aggregated systems, and also for pure MTS (with no phospholipid) and SPC liposomes. The results show (Fig. 8) that, from a general point of view, the pentacarbonyl complex is more toxic than the tetracarbonyl complex, as was in the case of the complexes of the L2 family.[17] When cell cultures were incubated with pure MTSs, the LC_{50} values were 148 ± 44 μM and 53 ± 0.03 μM for TCOL6 and PCOL6, respectively (calculated using the sigmoidal Hill equation). As regards the mixed TCOL6 systems, the most toxic aggregates were the TCOL6/SPC rods, with an LC_{50} value of 234 ± 14 μM. The TCOL6/SPC bicelles were less toxic, with an LC_{50} value of 421 ± 47 μM. In contrast, the vesicular PCOL6/SPC vesicles showed no toxicity, and the same cell viability as that of pure liposomes was obtained. The two types of vesicles obtained with PCOL6 exhibited a very different behaviour. While the stable to dilution aggregates were non-toxic in the studied range of concentrations, the unstable ones were highly toxic, with an LC_{50} value of 53 ± 0.1 μM, equivalent to that of the pure PCOL6 sample.

These results are consistent with toxicity being dependent on the type of the MTS aggregate. The critical micellar concentration of TCOL6 and PCOL6 is about 1 mM.[15,16] Thus, at all the concentrations of the viability study, the pure MTSs only exist as a monomer in the bulk, since the vesicles that they form in the stock solutions disaggregate once they are added to the cell incubation medium. The same is true for the NS-vesicles of PCOL6/SPC, which also partially disaggregate upon dilution and, thus, release free PCOL6 (Fig. 3). The three previous formulations exhibit the highest toxicity. In contrast, bicellar TCOL6/SPC aggregates are stable upon dilution, are about 8 nm in diameter, and exhibit an LC_{50} value higher than that of any one of the previously mentioned systems. Finally, the large and stable vesicles of TCOL6/SPC and PCOL6/SPC exhibited no toxicity in the studied range. This relationship between size/stability of the MTS aggregates and their toxicity is apparently broken by the toxicity of the TCOL6/SPC rods, which is higher than that of the bicelles, but it has to be taken into account that, as was previously stated, these very large structures rapidly sediment. Thus, rods are in close contact with the cells during the 24 h incubation and this should increase their toxicity.

Micro-FTIR spectroscopy of cells incubated with MTS aggregates

The main objective of the acquisition of micro-infrared spectra of cell cultures treated with mixed MTS/SPC systems was to determine to what extent the complexes could penetrate into the cells. This objective had the advantage of the strong IR absorption of the CO groups of the MTSs which, on the other hand, are not overlapped with any other absorption bands of the cell components. Principal Component Analysis (PCA) in the MTS CO region allowed the spectra to be classified according to the presence of MTS. The PCA results for the MTS CO region show a different distribution between the analysed systems (Fig. S4 and S5, ESI†). No outliers to the control (non-treated cells) were found for pure SPC liposomes, due to the absence of MTS CO bands. In the case of mixed TCOL6/SPC

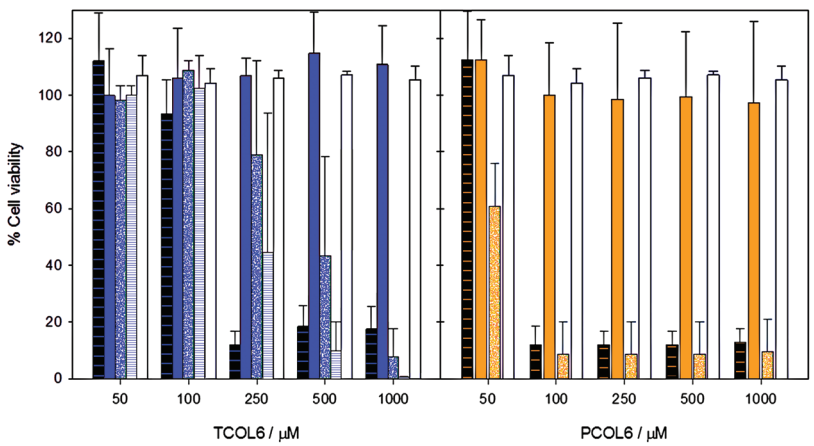

Fig. 8 Viability of human dermal fibroblasts after exposure for 12 h (mean ± std. dev.; $n \geq 4$) to TCOL6 (blue) or PCOL6 (orange). They were administered in free form (black dashed) or mixed with SPC as stable vesicles (blue or orange plain), bicelles (blue dotted), non-stable vesicles (orange dotted) or rods (blue dashed). The MTS to SPC molar ratios were 1 : 3 for TCOL6 and PCOL6 stable vesicles; 3 : 3 for TCOL6/SPC bicelles; 10 : 3 for PCOL6/SPC non-stable vesicles; and 10 : 3 for TCOL6/SPC rods. Pure SPC liposomes (white) were used as blanks and in these incubations SPC concentrations were the same as those of the respective treatments of mixtures of SPC and MTS.

systems, a significant number of outliers were found for vesicles only at 1000 μM (19%), bicelles (25%), and rods at 250 and 500 μM (94 and 99%, respectively), due to the absence of MTS CO bands. In contrast, all the checked PCOL6/SPC aggregates exhibited a large percentage of outliers. For the stable to dilution vesicles at 250 and 500 μM, they were about 85 and 76%, respectively, with the NS-vesicles showing 100%.

A relative estimation of the MTS interaction with the cells was obtained by the ratio between the area of one of the CO bands of the MTS and the amide I band located at 1650 cm^{-1}, which is proportional to the amount of protein in the cells. The results are shown in Fig. 9 and, as can be observed, the significant differences as regards the control (median comparison by the Mann–Whitney *U* test) were obtained with the same aggregated systems that provided significant outliers in the PCA. The data also show that the MTS internalisation is dependent on the type of aggregate, since bicelles, rods, and the NS-vesicles exhibit very high MTS to protein ratios compared with the other systems at equivalent concentrations.

Furthermore, this behaviour can be correlated with the toxicity assay. Observe that a high CO to protein ratio, which is indicative of high MTS internalisation (mean ratio higher than approximately 0.1), is exhibited by toxic aggregates (bicelles, rods and NS-vesicles). On the other hand, the other structures (large and stable to dilution vesicles of both MTSs) cause a smaller (but quantifiable) complex internalisation giving ratios below 0.05. Thus, these vesicles are good candidates to act as CO releasing systems, either by the non-toxic dose of internalised MTS, or by the MTS included in the mixed vesicles that surround the target cells. In both cases, light irradiation should trigger CO release and the gas should be delivered directly into the cells or to their surrounding medium.

Experimental section

General procedures

The preparations and manipulation of MTSs were performed under a nitrogen atmosphere using standard Schlenk tube techniques. All the solvents were dried and used freshly distilled. Tetrahydrofuran and methanol were distilled, respectively, over sodium/benzophenone and magnesium. Dichloromethane and acetonitrile were also distilled over sodium hydride, and all of them stored over 3 Å molecular sieves.

MTS preparation

MTSs $Mo(CO)_5L6$ (PCOL6) and $Mo(CO)_4L6$ (TCOL6) were prepared using previously reported methods.[15,16]

Preparation of mixed aggregates of phosphatidylcholine and MTSs by the thin film method

The appropriate volumes of chloroform/methanol (1 : 2 v/v) stock solutions of soybean phosphatidylcholine (SPC) and MTSs were mixed in order to achieve their desired final concentrations and molar ratios. The mixture was rotavapored and the homogeneous thin dry films obtained were kept under vacuum overnight. Subsequently the films were hydrated and the suspensions stirred for at least 30 minutes before any experiment.

Preparation of mixed aggregates of phosphatidylcholine and MTSs by microfluidification

Mixed aggregated MTS/SPC vesicles were obtained using a micromixer (moulded channels of 300 × 79 μm width × height) on a NanoAssemblr™ (Precision NanoSystems Inc., Vancouver,

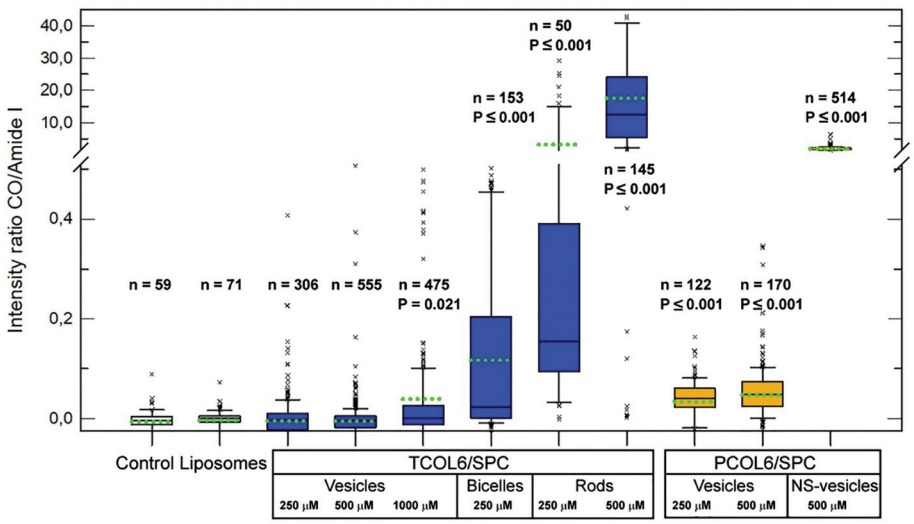

Fig. 9 Intensity ratio of the CO band of the MTS to the amide I band (cell protein) after treatment of cell cultures for 12 h with TCOL6/SPC or PCOL6/SPC aggregates at several concentrations. Black lines into the boxes represent the median, the green dotted lines are the mean and whiskers are the 9th and the 91st percentiles. Significant differences (*P*) of the median are shown below the number (*n*) of spectra acquired. The MTS to SPC molar ratios were 1 : 3 for TCOL6 and PCOL6 stable vesicles; 3 : 3 for TCOL6/SPC bicelles; 10 : 3 for PCOL6/SPC non-stable vesicles (NS-vesicles); and 10 : 3 for TCOL6/SPC rods.

Canada). SPC and MTS were dissolved at the desired concentration and molar ratio in ethanol or methanol, and the vesicles were obtained by injecting the solvent and an aqueous solution into the micromixer. The factors that were regulated are: the Flow Rate Ratio (FRR) between the aqueous and the solvent streams (aqueous/solvent from 1 to 5); the Total Flow Rate (TFR) of the solvent and aqueous streams (from 2 to 18 mL min^{-1}); and the ionic strength of the aqueous medium (from 0 to 155 mM of NaCl). To study the effect of FRR and TFR on the vesicle size a central composite design, complemented with perimetral level combinations, was used.[21] After processing the samples under the desired conditions the solvent was removed using size exclusion chromatography columns (Sephadex G-75) and the size distribution of the aggregates was measured by DLS. The relationship between the factors (FRR and TFR) and the response (mean diameter) was calculated by the stepwise method, fitting empirical, full second-order polynomial models that include constant, first-order, second-order, and interaction terms. After the correlations were carried out, the final equations contained only the significant parameters.

Dynamic light scattering measurements

The size distribution of the aggregates was measured by dynamic light scattering using an Ultrafine Particle Analyzer UPA150 (USA) or a Zetasizer 4 (Malvern Instruments, Malvern, UK). The results are expressed as volume distribution ($n \geq 3$).

Cryo-TEM and optical microscopy images

Transmission electron microscopy images were obtained at the Microscopy Services of the Universitat Autònoma de Barcelona using a Jeol JEM-1400 electron microscope operating at 120 kV. Optical microscopy pictures were acquired with an inverted phase contrast microscope IMT-2 Olympus, and samples were blotted onto a Neubauer chamber.

Monitorization of CO release by FTIR spectroscopy

Samples were exposed to UVA light (a Spectroline lamp; maximum wavelength intensity at 365 nm) or visible light (a Seon halogen lamp filtered with a Kodak Wraten 2B cut-off filter to eliminate any UV residual radiation) and, at different times, aliquots were taken and frozen at −80 °C. The evolution of the CO infrared bands of MTS upon irradiation was detected analyzing the aliquots with a Varian 660-IR FTIR spectrometer at the Laboratory of Luminescence and Biomolecular Spectroscopy of the Universitat Autònoma de Barcelona. Once defrozen, aliquots were blotted on IR windows and dried in a desiccator connected to a vacuum pump. The spectra (resolution 1 cm^{-1}; 50 scans) were normalized to the area of the SPC CO band at 1730 cm^{-1} (this group is not altered during irradiation) and the area ratios between the MTS CO (2071 cm^{-1} and 2019 cm^{-1} for PCOL6 and TCOL6, respectively) and SPC CO bands were obtained.

Toxicity studies

Cell viability of human dermal fibroblasts after incubation with different MTS/SPC systems was carried out by the XTT assay. The cells were seeded at a concentration of 7.5×10^4 cells per mL in DMEM 10% SBF and after confluence were maintained in DMEM 1% SBF for 24 h. Incubations with increasing concentrations of MTS suspensions diluted in cell medium (DMEM 1% SBF) were performed for 24 h. Subsequently, the medium was absorbed, the cells rinsed with PBS (0.1 mL) and the cell medium and the reagent were added. Absorbance at 450 nm was read after incubation for 4 h at 37 °C.

FTIR microscopy studies using synchrotron radiation

Internalization studies of MTS/SPC aggregates were carried out using human dermal fibroblasts cultured on infrared CaF_2 windows at 70% confluence. The samples were treated for 12 h with different formulations diluted in cell medium (DMEM 1% SBF) at the desired concentrations of MTS. A blank containing no MTS and 150 μM of SPC liposomes was included. Once the incubation medium was aspirated, the cells were rinsed three times with 0.5 mL of PBS and fixed with 0.5 mL of 4% paraformaldehyde for 30 minutes. After fixation the cells were rinsed with deionized water. The samples were observed with a Hyperion 3000 microscope equipped with a 36× magnification objective coupled to a Vertex 80 spectrometer (Bruker) at the MIRAS beamline at Alba Synchrotron (Catalunya, Spain).[28] The spectra were acquired with an optical window of 8×8 μm.

The presence of MTS in the spectra was detected performing Principal Component Analysis (PCA) of the region that contains the CO absorption bands of the MTS. After rejecting spectra with strong Mie scattering, a baseline correction was carried out, and the second derivative of the spectra was used to eliminate any baseline influence in the position of the peaks. The PCA plots allowed quantifying the percentage of outlier spectra of a given treatment referred to the control (non-treated ells). The relative amount of MTS in the cells was obtained by the ratio between the absorbance of a characteristic CO band of the MTS and that of the amide I band, corresponding to the cell protein.

Conclusions

We have demonstrated that, depending on their molar ratio, TCOL6 and PCOL6 can form several types of aggregated systems when mixed with phospholipids. Large vesicles, nanometric bicelles, and micrometre-sized rods are obtained, which shows a higher aggregate variability than that of the TCOL2 and PCOL2 systems. Thus, though the L6 family leads to the production of vesicles at low MTS/SPC ratios (as is the case with the L2 family), at high MTS/SPC ratios new structures are formed, like small bicelles, big rods and irregular vesicles. Therefore, the increase of the length of the hydrocarbon chain

has a relevant influence on the aggregation properties of the mixed MTS/SPC systems.

In a similar way to the L2 family, TCOL6 and PCOL6 mixed systems are also capable of releasing CO when activated by UVA and visible light. Among all of them, stable to dilution MTS/SPC vesicles appear to be a good candidate for further biomedical applications, since they cause a non-toxic internalisation of MTS into the cells.

Conflicts of interest

There are no conflicts to declare.

Acknowledgements

This work was supported by the Spanish MINECO-FEDER grants (BIO2015-67358-C2-2-P and CTQ2015-70371-REDT) and by the Generalitat de Catalunya (2014SGR-423 and 2017SGR-795). FTIR microscopy experiments were performed at MIRAS beamline at ALBA Synchrotron with the collaboration of ALBA staff.

Notes and references

1 (*a*) P. Scrimin, P. Tecilla, U. Tonellato and T. Vendrame, *J. Org. Chem.*, 1989, **54**, 5988–5991; (*b*) G. Ghirlanda, P. Scrimin, A. E. Kaifer and L. A. Echegoyen, *Langmuir*, 1996, **12**, 3695–3701; (*c*) I. A. Fallis, P. C. Griffiths, P. M. Griffiths, D. E. Hibbs, M. B. Hursthouse and A. L. Winnington, *Chem. Commun.*, 1998, **6**, 665–666; (*d*) E. Valls, J. Suades and R. Mathieu, *Organometallics*, 1999, **18**, 5475–5483.

2 G. Kaur, S. Kumar, N. Dilbaghi, B. Kaur, R. Kant, S. K. Guru, S. Bhushan and S. Jaglan, *Dalton Trans.*, 2016, **45**, 6582–6591.

3 I. A. Aiad, A. M. Badawi, M. M. El-Sukkary, A. A. El-Sawy and A. I. Adawy, *J. Surfactants Deterg.*, 2012, **15**, 223–234.

4 (*a*) B. Fell and G. Pagadogianakis, *J. Mol. Catal.*, 1991, **66**, 143–154; (*b*) H. Ding, B. E. Hanson and J. Bakos, *Angew. Chem., Int. Ed. Engl.*, 1995, **34**, 1645–1647; (*c*) H. Gulyas, P. Arva and J. Bakos, *Chem. Commun.*, 1997, **24**, 2385–2386; (*d*) M. S. Goedheijt, B. E. Hanson, J. N. H. Reek, P. C. J. Kamer and P. W. N. M. van Leeuwen, *J. Am. Chem. Soc.*, 2000, **122**, 1650–1657; (*e*) J. Li, Y. Tang, Q. Wang, X. Li, L. Cun, X. Zhang, J. Zhu, L. Li and J. Deng, *J. Am. Chem. Soc.*, 2012, **134**, 18522–18525; (*f*) R. D. Chakravarthy, V. Ramkumar and D. K. Chand, *Green Chem.*, 2014, **16**, 2190–2196; S. Gonawala, H. Baydoun, L. Wickramasinghe and C. N. Verani, *Chem. Commun.*, 2016, **52**, 8440–8443.

5 S. Gonawala, V. R. Leopoldino, K. Kpogo, C. Kenneth and C. N. Verani, *Chem. Commun.*, 2016, **52**, 11155–11158.

6 A. Mechler, B. D. Stringer, M. S. H. Mubin, E. H. Doeven, N. W. Phillips, J. Rudd-Schmidt and C. F. Hogan, *Biochim. Biophys. Acta, Biomembr.*, 2014, **1838**, 2939–2946.

7 H. N. Kagalwala, D. N. Chirdon, I. N. Mills, N. Budwal and S. Bernhard, *Inorg. Chem.*, 2017, **56**, 10162–10171.

8 (*a*) M. Vaccaro, G. Mangiapia, A. Radulescu, K. Schillén, G. D'Errico, G. Morelli and L. Paduano, *Soft Matter*, 2009, **5**, 2504–2512; (*b*) P. Gong, Z. Chen, Y. Chen, W. Wang, X. Wang and A. Hu, *Chem. Commun.*, 2011, **47**, 4240–4242; (*c*) Y. Chen, Q. Zhu, Y. Tian, W. Tang, F. Pan, R. Xiong, Y. Yuan and A. Hu, *Polym. Chem.*, 2015, **6**, 1521–1526; (*d*) Y. Chen, Q. Zhu, Y. Tian, W. Tang, F. Pan, R. Xiong, Y. Yuan and A. Hu, *Polym. Chem.*, 2015, **6**, 1521–1526.

9 (*a*) B. Donnio, *Curr. Opin. Colloid Interface Sci.*, 2002, **7**, 371–394; (*b*) M. Iida, M. Inoue, T. Tanase, T. Takeuchi, M. Sugibayashi and K. Ohta, *Eur. J. Inorg. Chem.*, 2004, **19**, 3920–3929; (*c*) T. Cardinaels, J. Ramaekers, K. Driesen, P. Nockemann, K. Van Hecke, L. Van Meervelt, B. Goderis and K. Binnemans, *Inorg. Chem.*, 2009, **48**, 2490–2499.

10 (*a*) M. Iida, C. Baba, M. Inoue, H. Yoshida, E. Taguchi and H. Furusho, *Chem. – Eur. J.*, 2008, **14**, 5047–5056; (*b*) S. Ye, Y. Liu, S. Chen, S. Liang, R. McHale, N. Ghasdian, Y. Lu and X. Wang, *Chem. Commun.*, 2011, **47**, 6831–6833; (*c*) X. Wang, Q. Yang, Y. Cao, H. Hao, J. Zhou and J. Hao, *Chem. – Eur. J.*, 2016, **22**, 17857–17865; (*d*) X. Wang, Q. Yang, Y. Cao, H. Hao, J. Zhou and J. Hao, *Chem. – Eur. J.*, 2016, **22**, 17857–17865; (*e*) R. Ohtani, T. Tokita, T. Takaya, K. Iwata, M. Kinoshita, N. Matsumori, M. Nakamura, L. F. Lindoyd and S. Hayami, *Chem. Commun.*, 2017, **53**, 13249–13252.

11 (*a*) H. D. Jayathilake, J. A. Driscoll, A. N. Bordenyuk, L. Wu, S. R. P. da Rocha, C. N. Verani and A. V. Benderskii, *Langmuir*, 2009, **25**, 6880–6886; (*b*) F. D. Lesh, M. M. Allard, R. Shanmugam, L. M. Hryhorczuk, J. F. Endicott, H. B. Schlegel and C. N. Verani, *Inorg. Chem.*, 2011, **50**, 969–977; (*c*) M. Mauro, G. De Paoli, M. Otter, D. Donghi, G. D'Alfonso and L. De Cola, *Dalton Trans.*, 2011, **40**, 12106–12116; (*d*) S. Joy, P. Pal, T. K. Mondal, G. B. Talapatra and S. Goswami, *Chem. – Eur. J.*, 2012, **18**, 1761–1771; (*e*) J. M. Fernandez-Hernandez, L. De Cola, H. J. Bolink, M. Clemente-Leon, E. Coronado, A. Forment-Aliaga, A. Lopez-Munoz and D. Repetto, *Langmuir*, 2014, **30**, 14021–14029.

12 (*a*) K. E. Amos, N. J. Brooks, N. C. King, S. Xie, J. Canales-Vázquez, M. J. Danks, H. B. Jervis, W. Zhou, J. M. Seddon and D. W. Bruce, *J. Mater. Chem.*, 2008, **18**, 5282–5292; (*b*) M. Botelho, J. Fernandez-Hernandez, T. Branquinho de Queiroz, H. Eckert, L. De Cola and A. de Camargo, *J. Mater. Chem.*, 2011, **21**, 8829–8834; (*c*) N. Hondow, J. Harowfield, G. Koutsantonis, G. Nealon and M. Saunders, *Microporous Mesoporous Mater.*, 2012, **151**, 264–270; (*d*) S. Kim, P. Durand, T. Roques-Carmes, J. Eastoe and A. Pasc, *Langmuir*, 2015, **31**, 1842–1849.

13 (*a*) P. C. Griffiths, I. A. Fallis, T. Chuenpratoom and R. Watanesk, *Adv. Colloid Interface Sci.*, 2006, **122**, 107–117; (*b*) S. Bhattacharya and N. Kumari, *Coord. Chem. Rev.*, 2009, **253**, 2133–2149; (*c*) F. Mancin, P. Scrimin, P. Tecilla and U. Tonellato, *Coord. Chem. Rev.*, 2009, **253**, 2150–

2165; (*d*) J. Zhang, X. Meng, X. Zeng and X. Yu, *Coord. Chem. Rev.*, 2009, **253**, 2166–2177; (*e*) T. Owen and A. Butler, *Coord. Chem. Rev.*, 2011, **255**, 678–687; (*f*) R. Kaur and S. K. Mehta, *Coord. Chem. Rev.*, 2014, **262**, 37–54.

14 (*a*) Z. Cheng, B. Ren, M. Gao, X. Liu and Z. Tong, *Macromolecules*, 2007, **40**, 7638–7643; (*b*) K. Tsuchiya, H. Yajima, H. Sakai and M. Abe, *Electrical Phenomena at Interfaces and Biointerfaces*, ed. H. Ohshima, John Wiley & Sons Inc., Hoboken, NJ, 2012, pp. 567–582.

15 E. Parera, F. Comelles, R. Barnadas and J. Suades, *Chem. Commun.*, 2011, **47**, 4460–4462.

16 E. Parera, M. Marín-García, R. Pons, F. Comelles, J. Suades and R. Barnadas-Rodríguez, *Organometallics*, 2016, **35**, 484–493.

17 M. Marín-García, N. Benseny-Cases, M. Camacho, J. Suades and R. Barnadas-Rodríguez, *Chem. Commun.*, 2017, **53**, 8455–8458.

18 (*a*) J. F. Hainfeld, F. R. Furuya and R. D. Powell, *J. Struct. Biol.*, 1999, **127**(2), 152–160; (*b*) K. Osada, H. Cabral, Y. Mochida, S. Lee, K. Nagata, T. Matsuura, M. Yamamoto, Y. Anraku, A. Kishimura, N. Nishiyama and K. Kataoka, *J. Am. Chem. Soc.*, 2012, **134**, 13172–13175; (*c*) P. Garg, G. Kaur, G. R. Chaudhary, S. L. Gawalib and P. A. Hassan, *Phys. Chem. Chem. Phys.*, 2017, **19**, 25764–25773.

19 M. Almgren, K. Edwards and G. Karlsson, *Colloids Surf., A*, 2000, **174**, 3–21.

20 K. Edwards, M. Johnsson, G. Karlsson and M. Silvander, *Biophys. J.*, 1997, **73**, 258–266.

21 (*a*) R. Barnadas-Rodríguez and M. Sabés, *Int. J. Pharm.*, 2001, **213**, 175–186; (*b*) R. Barnadas-Rodríguez and M. Sabés, *Methods Enzymol.*, 2003, **367**, 28–46.

22 (*a*) A. Jahn, W. N. Vreeland, D. L. DeVoe, L. E. Locascio and M. Gaitan, *Langmuir*, 2007, **23**, 6289–6293; (*b*) D. Carugo, E. Bottaro, J. Owen, E. Stride and Cl. Nastruzzi, *Sci. Rep.*, 2016, **6**, 25876, DOI: 10.1038/srep25876; (*c*) K. Nagarsekar, M. Ashtikar, F. Steiniger, J. Thamm, F. H. Schacher and A. Fahr, *J. Liposome Res.*, 2017, **27**(1), 32–40.

23 (*a*) J. S. Hong, S. M. Stavis, S. H. DePaoli Lacerda, L. E. Locascio, S. R. Raghavan and M. Gaitan, *Langmuir*, 2010, **26**(13), 11581–11588; (*b*) M. Mijajlovic, D. Wright, V. Zivkovic, J. X. Bi and M. J. Biggs, *Colloids Surf., B*, 2013, **104**, 276–281; (*c*) Y.-D. Dong, E. Tchung, C. Nowell, S. Kaga, N. Leong, D. Mehta, L. M. Kaminskas and B. J. Boyd, *J. Liposome Res.*, 2017, **20**, 1–9, DOI: 10.1080/08982104.2017.1391285; (*d*) E. Kastner, V. Verma, D. Lowry and Y. Perrie, *Int. J. Pharm.*, 2015, **485**, 122–130; (*e*) E. Kastner, R. Kaur, D. Lowry, B. Moghaddam, A. Wilkinson and Y. Perrie, *Int. J. Pharm.*, 2015, **477**, 361–368.

24 I. V. Zhigaltsev, N. Belliveau, I. Hafez, A. K. K. Leung, J. Huft, C. Hansen and P. R. Cullis, *Langmuir*, 2012, **28**, 3633–3640.

25 (*a*) H. V. Ly, D. E. Block and M. L. Longo, *Langmuir*, 2002, **18**(23), 8988–8995; (*b*) Y.-M. Yang, K.-C. Wu, Z.-L. Huang and C.-H. Chang, *Langmuir*, 2008, **24**, 1695–1700.

26 J. Paxman, B. Hunt, D. Hallan, S. R. Zarbock and D. J. Woodbury, *Biophys. J.*, 2017, **112**, 121–132.

27 (*a*) R. Motterlini and L. E. Otterbein, *Nat. Rev. Drug Discovery*, 2010, **9**, 728–743; (*b*) S. García-Gallego and G. J. L. Bernardes, *Angew. Chem., Int. Ed.*, 2014, **53**, 9712–9721.

28 I. Yousef, L. Ribó, A. Crisol, I. Šics, E. Ellis, T. Ducic, M. Kreuzer, N. Benseny-Cases, M. Quispe, P. Dumas, S. Lefrançois, T. Moreno, G. García, S. Ferrer, J. Nicolas and M. A. G. Aranda, *Synchrotron Radiat. News*, 2017, **30**, 4–6.